Inorganic Chemistry

Article

pubs.acs.org/IC

Tuning of Water and Hydroxide Content of Intercalated Ruddlesden–Popper-type Oxides in the $PrSr_3Co_{1.5}Fe_{1.5}O_{10-\delta}$ System

Laurent Jantsky, Hiroshi Okamoto, Antoine Demont,† and Helmer Fjellvåg*

Centre for Materials Science and Nanotechnology, Department of Chemistry, University of Oslo, P.O. Box 1033, Blindern, N-0315 Oslo, Norway

Supporting Information

ABSTRACT: A series of hydration experiments of the Ruddlesden–Popper phase $PrSr_3Co_{1.5}Fe_{1.5}O_{10-\delta}$ with varying levels of oxygen nonstoichiometry were performed with the goal to clarify phase formation and underlying mechanisms and driving forces. The hydration reaction is most intense for partly reduced samples with a vacancy concentration corresponding to $\delta \approx 1$. Fully oxidized samples show little or no tendency toward hydration. Presence of oxygen vacancies acts as a prerequisite for hydration. Probably, the basicity of the materials owing to A-site cations is another contributing factor to the hydration ability. Under CO_2 free conditions pure hydrates and oxide hydroxides are formed. In CO_2-containing atmosphere, additional carbonate anions are easily incorporated into the hydrate, probably at the expense of hydroxyl groups. The *I*-centered $PrSr_3Co_{1.5}Fe_{1.5}O_8(OH)_2 \cdot 1H_2O$ achieves a highly expanded *c*-axis upon the topochemical insertion reactions. In situ powder synchrotron X-ray diffraction (SXRD) shows that the hydrate converts to an oxide hydroxide, $PrSr_3Co_{1.5}Fe_{1.5}O_8(OH)_2$, at 70 °C with a primitive orthorhombic unit cell. Upon heating above 170 °C, an *I*-centered product is formed for which further dehydroxylation occurs at around 400–500 °C. Rietveld refinement of SXRD data shows that the absorbed water molecules fill the tetrahedral voids of the $[AO]^{RS}$ rock salt layer of the monoclinic hydrate.

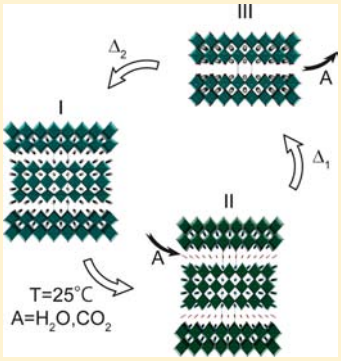

INTRODUCTION

Ruddlesden–Popper (RP) type phases $A_{n+1}B_nO_{3n+1}$ are formally described as intergrowths of rock salt (RS) and perovskite (P) type slabs of $[AO]^{RS}$–$n[ABO_3]^P$ along [001].[1,2] Several RP and related Dion–Jacobson (DJ) phases[3] with, *inter alia*, TiO_6, NbO_6, and TaO_6 building units undergo ion exchange and incorporate water into the $[AO]^{RS}$ slab subsequent to exchange of alkali cations by protons.[4,5] This ability to incorporate water is astounding since the 2D-structural motifs of the crystal structures hardly reflect any weak chemical bonds within the $[AO]^{RS}$ slabs.

RP3 ferrites like $NdSr_3Fe_3O_{9-\delta}$ and $PrSr_3Fe_{1.5}Co_{1.5}O_{10-\delta}$[6] exhibit large oxygen nonstoichiometries under reductive atmospheres with the vacancies mainly located in the central $FeO_{2-\delta}$ plane of the triple perovskite $[(Sr/Nd)(Fe/Co)O_{3-\delta}]_3^P$ slab.[7] $NdSr_3Fe_3O_{9-\delta}$ is reported to react with ambient moisture and undergo a reversible topotactic hydrolysis and hydration reaction, forming a hydrated oxide hydroxide phase with novel stacking elements along the *c*-axis, that is, $[SrO_{0.5}(OH)_{0.5}$–OH/H_2O–$SrO_{0.5}(OH)_{0.5}]^{RS}$, as compared with $[SrO–SrO]^{RS}$ for the original RP3 oxide. Interestingly, this hydrated oxide hydroxide transforms to an oxide hydroxide $NdSr_3Fe_3O_{7.5}(OH)_2$ on heating at around 100 °C. Upon further heating, dehydroxylation occurs and restores the original $NdSr_3Fe_3O_{9-\delta}$ oxide. Similarly hydrated oxide hydroxide phases are known for Co-based RP phases like $Sr_3Co_2O_5(OH)_2 \cdot xH_2O$, $Sr_3Co_{1.7}Ti_{0.3}O_5(OH)_2 \cdot xH_2O$, and $Sr_4Co_{1.6}Ti_{1.4}O_8$.[8,9] The chemical formulas for the various phases can be generalized $A_{n+1}B_nO_{3n-1-\delta}(OH)_2 \cdot nH_2O$, $A_{n+1}B_nO_{3n-1-\delta}(OH)_2$, and $A_{n+1}B_nO_{3n+1-\delta}$ (A = alkaline earth or rare earth; B = Ti, Mn, Fe, Co, or Ni). These phases are below termed hydrated oxide hydroxide, oxide hydroxide, and oxide, respectively.

Oxygen nonstoichiometry combined with hydration ability has further been reported for the RP2 ferrite $Sr_3Fe_2O_{7-\delta}$ by Matvetjeff et al.[10] For a water-containing phase, they discussed whether oxonium ions (protons) exist according to the formula $Sr_3Fe_2O_{6.3}(H_3O)_{0.4} \cdot 1.6H_2O$ rather than $Sr_3Fe_2O_{5.9}(OH)_{0.4} \cdot 2H_2O$, assuming a fixed Fe oxidation state. Increased amounts of oxygen vacancies have a positive impact on the hydration, possibly due to kinetics.

The topotactic hydrations of RP-type and layer-like oxides more generally provide an intriguing playground for modifying and tuning physical properties, examples being photocatalytic decomposition of water by $K_2Ln_2Ti_3O_{10}$ (Ln, lanthanide),[11] proton conduction through hydrogen-bonded network of intercalated water in $HLa_2NdTi_2O_{10} \cdot 1.5H_2O$, and superconductivity in $Na_xCoO_2 \cdot yH_2O$.[12] Physical properties are further readily modified by (heterovalent) substitutions and introduction of vacancies. For example, cobalt substitution for B-site iron in perovskite and RP type phases typically enhances electronic and ionic conductivities, $(La,Sr)(Fe,Co)O_3$ and $Sr_3(Fe,Co)_2O_{7-\delta}$.[13−15] For $Sr_4Fe_3O_{10}$,[16] enhanced oxygen

Received: January 1, 2012
Published: August 20, 2012

   dx.doi.org/10.1021/ic300001s | Inorg. Chem. 2012, 51, 9181–9191

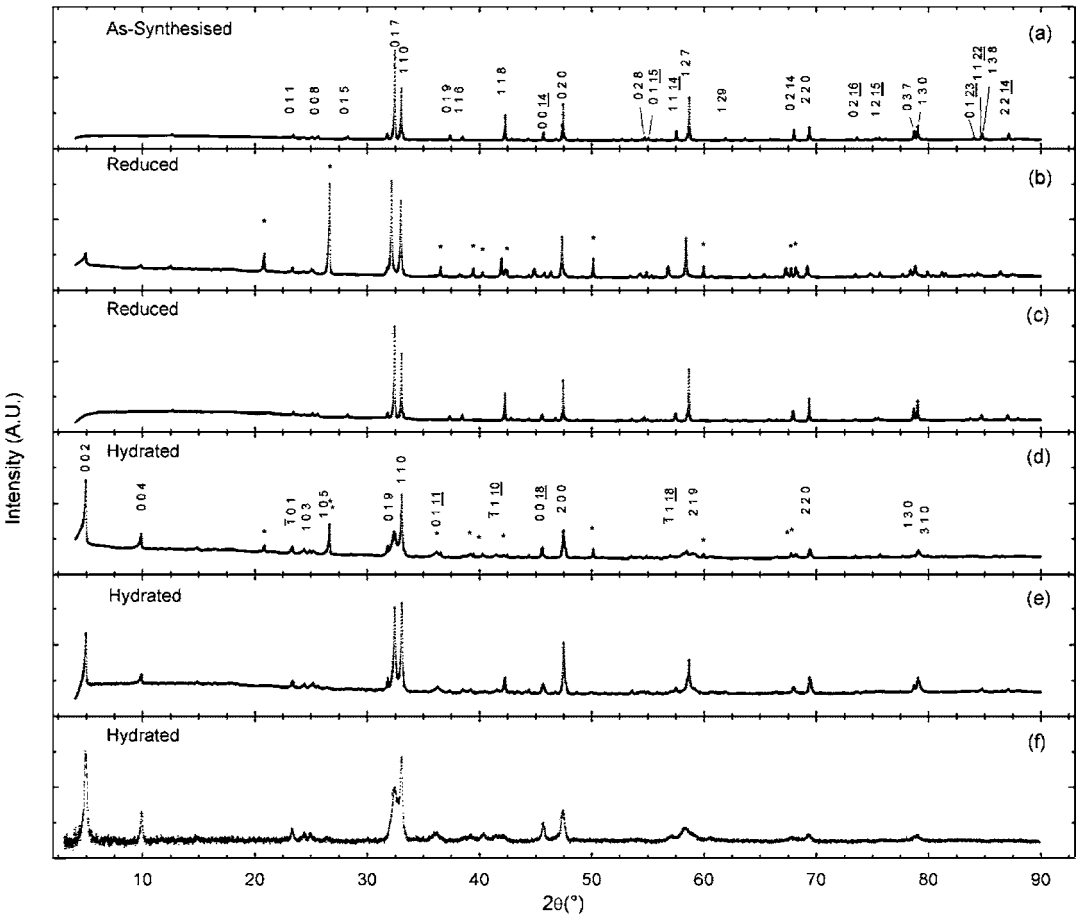

Figure 1. PXD patterns of (a) as-synthesized $PrSr_3Co_{1.5}Fe_{1.5}O_{10-\delta}$, samples postannealed (b) at 700 °C in N_2 and (c) at 250 °C in H_2, (d) sample b subjected to a water bath for 10 h, (e) sample c similarly treated for 10 h, and (f) sample c subjected to 3 weeks ambient atmosphere. Peaks denoted by ∗ are due to SiO_2 internal standard. Miller indices are given for selected reflections in parts a and d.

nonstoichiometry is achieved via heterovalent La(III)-for-Sr(II) substitution,[17] whereas in Co-based RP-phases like $La_4Co_3O_{10\pm\delta}$, extended oxygen nonstoichiometry and vacancy ordering is reported for reduced phases.[18,19]

Previously, we reported on the crystal structure of RP3-phase $PrSr_3Co_{1.5}Fe_{1.5}O_{10-\delta}$.[6] The Co atoms showed a weak preference to be located in the central $[(Ln,Sr)(Fe,Co)O_3]^P$ slab. Upon reduction, oxygen vacancies appear, primarily within these $[(Ln,Sr)(Fe,Co)O_3]^P$ slabs. Because there is no ordering of the A cations, the $[AO]^{RS}$ slab achieves formally a positive charge, whereas the $[ABO_3]^P$ block achieves a negative charge. The creation of vacancies in the P-slab is compensated by reduction of the B cations.

In the present study, the hydration behavior of the RP3-phase $PrSr_3Co_{1.5}Fe_{1.5}O_{10-\delta}$ is carefully investigated with the aim to shed light on open issues: the role of oxygen vacancies for the ability to hydrate; hydration capacity as function of oxygen nonstoichiometry; hydration mechanism; role of oxidative potential of B-site cations; description of stability, composition, and structure for involved phases at various levels of hydration (soft and rough conditions in air). Based on $PrSr_3Co_{1.5}Fe_{1.5}O_{10-\delta}$ treated in air, annealings in different conditions were carried out to clarify the effect of oxygen nonstoichiometry on the topotactic hydration reactions. The reverse process, that is, topotactic deintercalation and dehydroxylation, is discussed on the basis of in situ high temperature synchrotron powder diffraction data (SXRD) data. A rationale for the hydration behavior is provided on the basis of thermal analysis data, cerimetric titrations, and crystal structure data from Rietveld refinements of SXRD data.

EXPERIMENTAL SECTION

Samples of $PrSr_3Co_{1.5}Fe_{1.5}O_{10-\delta}$ were prepared from a master batch of precursor powder, synthesized from $Sr(NO_3)_2$ (Riedel de Haën, puriss p.a. ACS reagent 99%), $Pr(NO_3)_3{\cdot}6H_2O$ (Aldrich 99.9%), Fe metal (Goodfellow 99.99%), and Co metal (Chempur Electrolytic 99.9%). The reactants were dissolved in concentrated nitric acid and thereafter added to a citric acid melt and dried overnight at 300 °C before being calcined at 500 °C in a muffle furnace. Pellets were pressed from the precursor powder and reacted at 1050 and 1250 °C for 15 and 25 h, respectively. The final firing was performed at 1350 °C for 24 h in air. To ensure full oxidation, the samples were crushed and postannealed in oxygen at 250 °C for 5−7 days. Oxygen-deficient $PrSr_3Co_{1.5}Fe_{1.5}O_{10-\delta}$ samples were obtained by postannealing for 15 h under mildly reductive atmospheres of N_2 (99.99%) at 300, 500, 700, and 900 °C, yielding oxygen contents $10-\delta > 9.0$. Lower oxygen contents, $10-\delta < 9.0$, were obtained through heat treatments in 10% H_2−90% Ar at 250, 300, and 500 °C for 12 h. The oxygen contents of selected samples were determined by cerimetric titration using cerium(IV) sulfate in acidic solution, thereby providing data for the average oxidation state of $Co_{1.5}Fe_{1.5}$. The dissolution of the sample was carried out under a flow of inert gas (N_2 or Ar) in a degassed 1 M HCl solution.[20] Hydrated oxide hydroxides were readily obtained by subjecting postannealed $PrSr_3Co_{1.5}Fe_{1.5}O_{10-\delta}$ samples to moist air (25 °C and relative humidity 40−60%) over a period of days to weeks.[21] Accelerated hydration was achieved by suspending the samples above a water bath kept at 80 °C for several hours. Characteristics connected

dx.doi.org/10.1021/ic300001s | Inorg. Chem. 2012, 51, 9181−9191

with water uptake or release, oxidation and reduction, and total oxygen content analysis were derived through TG experiments (Perkin-Elmer, Pyris 1 TGA) in O_2, N_2, or 5% H_2−95% Ar atmospheres. The sample masses were in the range 20−70 mg with heating rates of 1−10 °C/min.

Phase content and unit cell dimensions were derived from conventional powder X-ray diffraction (PXD) using monochromatized Cu Kα_1 radiation and either a Huber G670 instrument equipped with a 1D-detector or a Siemens D5000 equipped with a Braun PSD detector.

In-situ SXRD data were collected at the BM01A beamline (SNBL) at the European Synchrotron Radiation Facility (ESRF). Data were collected using a 2D-detector MAR345, exposure time 20 s and readout time 1.45 min. Temperatures were varied between ambient and 400 °C at a heating rate of 3 °C/min. The adopted wavelength was 0.70417 Å. The 2D diffraction data were rebinned into 1D (intensity versus 2θ) sets with an equivalent 2θ step size of 0.0227° using the Fit2D program.[22] These data were subsequently analyzed for the range $1.85° \leq 2\theta \leq 35.5°$. Unit cell dimensions and atomic coordinates were derived from refinements according to the Rietveld method[23] using the Fullprof code.[24] Scale factor, zero point, pseudo-Voigt profile parameters, unit cell dimensions, positional parameters, and isotropic displacement factors entered into the final least-squares refinements. Furthermore, soft constraints on the interatomic distances were added (i.e., $d_{B-O} = 1.93 \pm 0.1$ Å and $d_{B-OH} = 2.00 \pm 0.15$ Å) to ensure meaningful positional parameters. The variation interval was determined by considering the sum of the oxygen ionic radius with that of the transition metal in reasonable oxidation states and coordination environments. Bond valence calculations were performed using the BondStr GUI[24] integrated in the Fullprof suite. Additional atoms, that is, absorbed water molecules, were located by means of difference Fourier synthesis maps according to the GFOUR code.[24]

Fourier transform infrared spectroscopy (FTIR) was performed using a Perkin-Elmer system 2000 FTIR spectrometer. Spectra were collected for the oxidized $PrSr_3Fe_{1.5}Co_{1.5}O_{10-\delta}$ on mildly (15 h) and aggressively (4 h) hydrated samples of a reduced phase as well as for selected binary oxides and carbonates ($SrCO_3$ Fluka >98%, $BaCO_3$ Fluka purum P.A. >98.5%, Fe_2O_3 Strem chemicals 99.8%, and Co_3O_4 JT Baker analyzed reagent 70−74% Co) in air. The latter spectra were used as reference patterns. Some 2 mg of reference materials or 5 mg of sample were ground together with ca. 200 mg of KBr, then pelletized into discs of 10 mm diameter. Spectra were collected for reference materials and fully oxidized RP3 between 7800 and 370 cm^{-1} with 4 cm^{-1} steps. For the two hydrated samples, spectra were collected between 6000 and 370 cm^{-1} with 2 cm^{-1} steps.

RESULTS

Hydrate Formation as a Function of Oxygen Nonstoichiometry. The XRD pattern for the as-synthesized $PrSr_3Co_{1.5}Fe_{1.5}O_{10-\delta}$ confirmed a pure RP3 phase, see Figure 1a. The tetragonal unit cell dimensions are in good agreement with previous data,[15] space group *I*4/*mmm*; $a \approx 3.827$ Å and $c \approx 27.76$ Å. Cerimetric titrations gave an oxygen content of $10-\delta = 9.910(4)$ for the fully oxidized sample. For this tetragonal phase, earlier work showed that oxygen vacancies are predominantly located in the [(Fe,Co)O_2] layers in the middle of the (triple) perovskite block (see ref 6.). Considering this as the dominant vacancy mechanism, the cerimetrically determined stoichiometry corresponds to 4.5% of these O-sites being vacant. This almost fully oxygenated phase shows no reaction with water.

However, $PrSr_3Co_{1.5}Fe_{1.5}O_{10-\delta}$ exists over a wide range of oxygen stoichiometries attainable upon annealing in controlled atmospheres, by the use of oxygen getters, etc. Supposing that the reactivity toward humidity and the ability to form hydrates and hydroxides may be enhanced by the presence of anion vacancies, the relationship between structure, nonstoichiometry, average oxidation state, and ability to react with H_2O under hydrate formation was examined by exposing samples with variable oxygen stoichiometries to water vapor. Reduced oxides with compositions $8.20 \leq 10-\delta < 9.91$ were prepared by postannealing of the fully oxidized $O_{9.91}$ sample under carefully selected atmospheres and thermal treatment. The adopted conditions and achieved oxygen contents according to TG analyses are listed in Table 1.

Table 1. Oxygen Content for Various Annealing Schemes and Methods Used for Determination

atm.	temp (°C)	duration	oxygen content	method
O_2	250	days	$O_{9.91}$	cerimetry
N_2	300	15 h	$O_{9.73}$	TG
	500	11 h	$O_{9.29}$	TG
	700	5 h	$O_{9.10}$	TG
	900	5 h	$O_{9.00}$	TG
H_2	250	12 h	$O_{8.9}$	TG
	350	12 h	$O_{8.52}$	TG
	500	12 h	$O_{8.22}$	TG

The *I*4/*mmm* symmetry of the $PrSr_3Co_{1.5}Fe_{1.5}O_{9.91}$ is retained for the reduced oxide samples, except for $O_{9.00}$, where peak splitting in the PXD pattern indicatesorthorhombic distortion. The variation in unit cell dimensions versus oxygen content is shown in Figure 2. The volume increases as expected with increasing nonstoichiometry (i.e., larger size of B-site

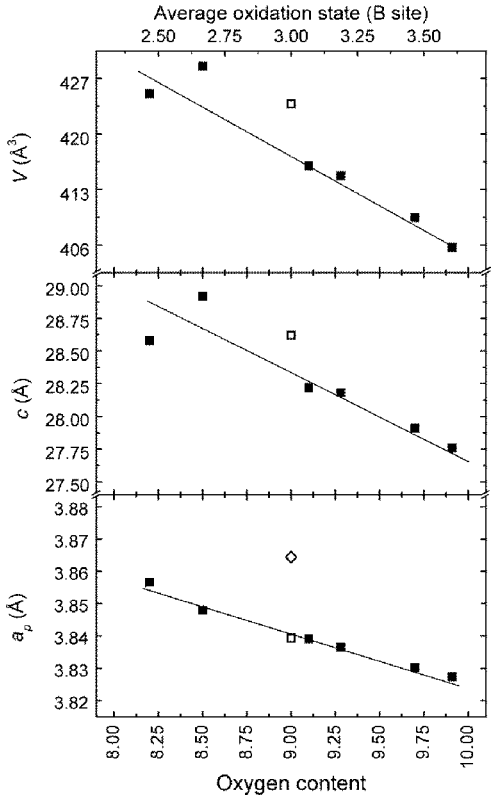

Figure 2. Unit cell dimensions as function of oxygen nonstoichiometry (lower axis) and of corresponding average B-site oxidation state (upper axis) for $PrSr_3Fe_{1.5}Co_{1.5}O_{10-\delta}$ (*I*4/*mmm*). Dimensions for orthorhombically distorted $O_{9.00}$ are given in terms of a (□) and b (◇).

dx.doi.org/10.1021/ic300001s | Inorg. Chem. 2012, 51, 9181−9191

cations; less volume efficient packings). The orthorhombic distortion for $O_{9.00}$ fits with situations frequently encountered for perovskite-related oxides, caused by, for example, octahedra tilting due to chemical pressure and size mismatch of A and B cations, spin, charge, and orbital ordering, or ordering of oxygen vacancies. Because the sizes of the Pr^{3+} and Nd^{3+} cations, as well as Fe^{3+} and Co^{3+}, are similar, we expect similar orderings of oxygen vacancies in $PrSr_3Co_{1.5}Fe_{1.5}O_9$ and the earlier studied $NdSr_3Fe_3O_9$. The XRD pattern obtained for the $O_{9.00}$ composition could be readily indexed in the *Cmcm* (no. 63) space group, which is equivalent to that of the Nd phase (i.e., *Bbmm*; ICSD no. 172509) reported by Barrier et al.[25] See Supporting Information Figure IV.

Samples with oxygen stoichiometries between $O_{8.22}$ and $O_{9.91}$ were exposed to humidity for up to 10 h above a water bath maintained at 80 °C. Figure 1 shows representative PXD patterns before and after exposure to humid air. Note that Figure 1f corresponds to the samples in Figure 1c,e subjected to ambient atmosphere for 3 weeks rather than humidity at 80 °C.

Two observations are evident from the PXD data in Figure 1: (i) growing intensity of (002) at $2\Theta \approx 5°$ of the hydrated oxide hydroxide phase with increasing exposure time to humidity and (ii) the broadening of the *h*0*l* reflections of the hydrate phase. The latter was explained by a monoclinic distortion, which in particular is supported by shoulders and splittings of reflections in the "(109)−(110)" group for the hydrated oxide hydroxide phase. Undisputed evidence would require a combination of electron diffraction (TEM) and high-resolution powder diffraction data. TEM data for these hydrated phases is known to be difficult to collect due to water loss in high vacuum under intense electron beams.[7,8] High-resolution X-ray synchrotron data are currently under investigation.

Intercalation of layered materials is typically accompanied by a structural expansion perpendicular to the layers, as is indeed observed. For the current RP3 phase, the hydration results in a well-defined phase with elongated *c*-axis. The degree of *c*-axis expansion reflects the type of incorporated species, OH versus OH plus H_2O. The appearance of Bragg reflections at low 2θ angles in Figure 1b,d−f is consistent with an elongated *c*-axis of some 4 Å compared with the basic RP3 oxide as expected for water inserted into $[AO]^{RS}$ layers.[7,9,21,26,27] Based on refined unit cell dimensions, the height of the individual RS layers are 6.2 and 4.7 Å for the two basic variants achieved currently, that is, hydrated oxide hydroxide and oxide hydroxide, respectively. These values can be compared with 6.2 and 4.6 Å expansions in the hydrated oxide hydroxide and oxide hydroxide forms of $NdSr_3Fe_3O_{8.5}$.

Ex-situ PXD data for variously hydrated samples show the presence of a monoclinic phase. Unit cell dimensions were derived by profile fitting on a primitive monoclinic lattice, yielding $a \approx 3.846$ Å, $b \approx 3.849$ Å, $c \approx 35.82$ Å, and $\beta \approx 88.85°$ (see details below) for the hydrated oxide hydroxide. The intensity of $(002)_{hydr}$ at $2\theta \approx 5°$ was used as measure of the degree of specimen hydration, normalized to $I(107)_{ox}$ (the most intense peak of the parent oxide at $2\theta \approx 32°$). $I(002)_{hydr}/I(107)_{ox}$ is plotted versus exposure time to humid atmosphere in Figure 3a for samples with oxygen stoichiometries between $O_{8.22}$ and $O_{9.73}$. These data show a correlation between the ability to hydrate and rate of hydration and the RP3 oxygen nonstoichiometry. There appears to exist an optimum non-stoichiometry around $O_{9.0}$ with respect to hydration. At higher oxygen contents, the RP3 phase is less facile to hydrate. Also for the most reduced sample the ability to hydrate is low.

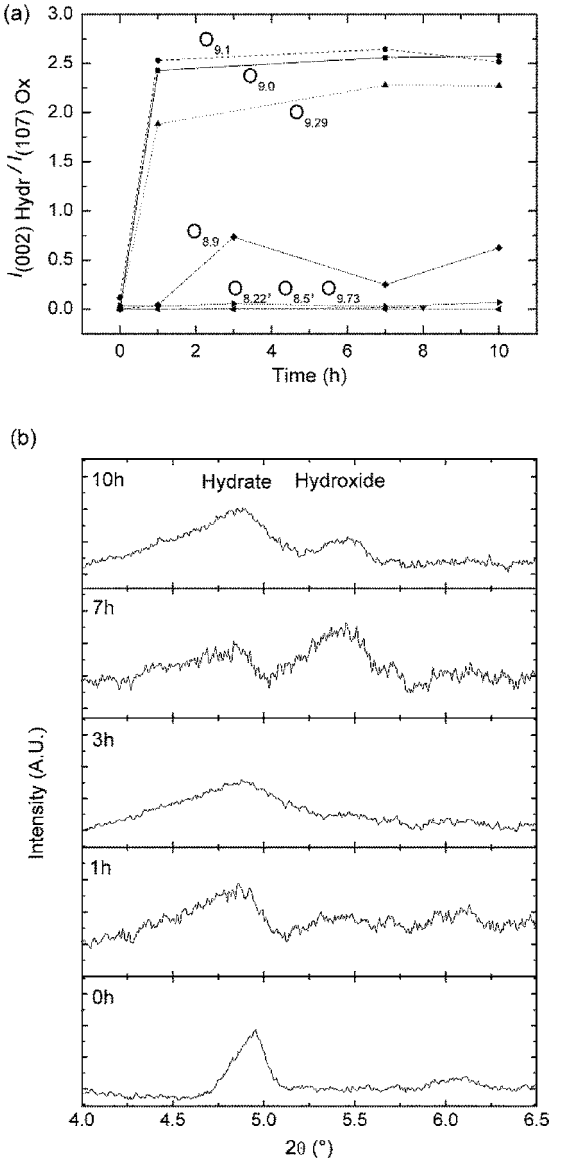

Figure 3. (a) Degree of hydration as function of exposure time to humidity for samples with different oxygen nonstoichiometries. (b) Low-angle diffraction region ($4° < 2 < 6.5°$) for $PrSr_3Fe_{1.5}Co_{1.5}O_{8.52}$ showing presence of both hydrate and hydroxide phases before and during exposure to water vapor at 80 °C. Initial presence of hydrate suggests rapid hydration under atmospheric conditions.

For $PrSr_3Co_{1.5}Fe_{1.5}O_{8.52}$ (postannealed at 350 °C in H_2), the hydrate oxide hydroxide and the oxide hydroxide form simultaneously during the hydration process at 80 °C [see Figure 3(b)] as evidenced by two low angle diffraction peaks at $2\theta \approx 5.0°$ and 5.5°, corresponding to, respectively, $(002)_{hydr}$ and $(001)_{hydrox}$ for the hydrate and the oxide hydroxide. The observation of a sharp hydrate peak within a few minutes of hydration indicates that atmospheric hydration is extremely fast and that inert handling would be required for safe keeping of the oxide precursor. The observation of two products at 80 °C indicate either a two-step process or a limited stability window for the hydrate with onset of thermal decomposition into an oxide hydroxide around 80 °C in humid air.

PXD data for $PrSr_3Co_{1.5}Fe_{1.5}O_{8.22}$ (postannealed in H_2 at 500 °C) showed peak splitting of $(107)_{ox}$ and $(110)_{ox}$. This is interpreted to evidence sample decomposition by reduction

dx.doi.org/10.1021/ic300001s | *Inorg. Chem.* 2012, 51, 9181−9191

beyond the stability window. Supporting evidence was obtained upon exposure to humid air at 80 °C. Additional reflections to those of RP3 derivatives are observed and ascribed to a reduced oxide with Brownmillerite structure and to a hydroxide garnet similar to $Sr_3Fe_2(OH)_{12}$ as reported by Ito et al.[28] and Matvejeff et al. during hydration of $Sr_{n+1}Fe_nO_{(3n+1)-\delta}$.[10] In a few experiments, for example, one run for $PrSr_3Co_{1.5}Fe_{1.5}O_{9.00}$, sample surfaces changed from black to white during hydration. Nevertheless, the PXD patterns showed no evidence for crystalline impurities. This suggests that leaching may occur upon hydration, possibly giving amorphous $Sr(OH)_2/SrCO_3$ at surfaces.

Figure 4 shows the degree of hydration in humid air at 80 °C (cf Table 1) versus oxygen content as evaluated from relative

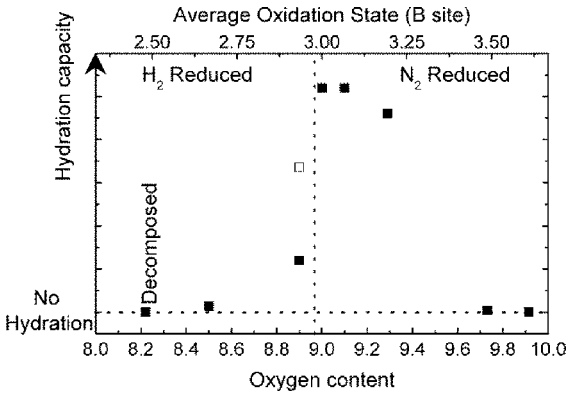

Figure 4. Degree of hydration at 80 °C in humid air as measured from diffraction data versus oxygen composition (nonstoichiometry), see text for details. Open symbol for $O_{8.9}$ refers to hydration at ambient temperature. Average oxidation state of the B site cations shown on upper horizontal axis.

intensities of the strong $(107)_{ox}$ and $(002)_{hydr}$ peaks. Maximum hydration occurs for oxygen stoichiometries around O_9. The behavior depends on temperature and atmosphere, with $p(H_2O)$ being a key parameter. However, it was also proven that $p(CO_2)$ affects the reaction process, see below. The temperature dependence is evident; the low degree of hydration at 80 °C for oxygen stoichiometries less than O_9 becomes enhanced in moist air at ambient temperature, compare data for $O_{8.9}$ forcefully hydrated at 80 °C and in air at ambient in Figure 4.

The thermal stability of the hydrated products was investigated by TGA. Figure 5 shows weight changes upon heating in N_2 up to 900 °C. The weight changes were normalized by subsequent conversion to the fully oxidized $O_{9.91}$ composition by heating in O_2 at 250 °C. As shown in Figure 5a for samples subjected to accelerated hydration at 80 °C, the observed total weight loss varies smoothly with the oxygen content of the RP3 oxide precursor and increases upon varying the oxygen stoichiometry from $O_{9.7}$ to $O_{9.00}$ There are clear indications for plateaus in all TG curves; however, the steps are rather blurred, Figure 5a. The weight loss is completed at rather elevated temperatures, some 700−900 °C. Whereas the total weight loss correlates with the initial RP3 oxygen content, no such correlation exists for the losses in the intermediate temperature regime, that is, 250 < T < 500 °C. More distinct features are observed for samples hydrated at ambient temperature, Figure 5b. Here, a plateau develops around 80 °C before a second weight loss sets in for temperatures up to

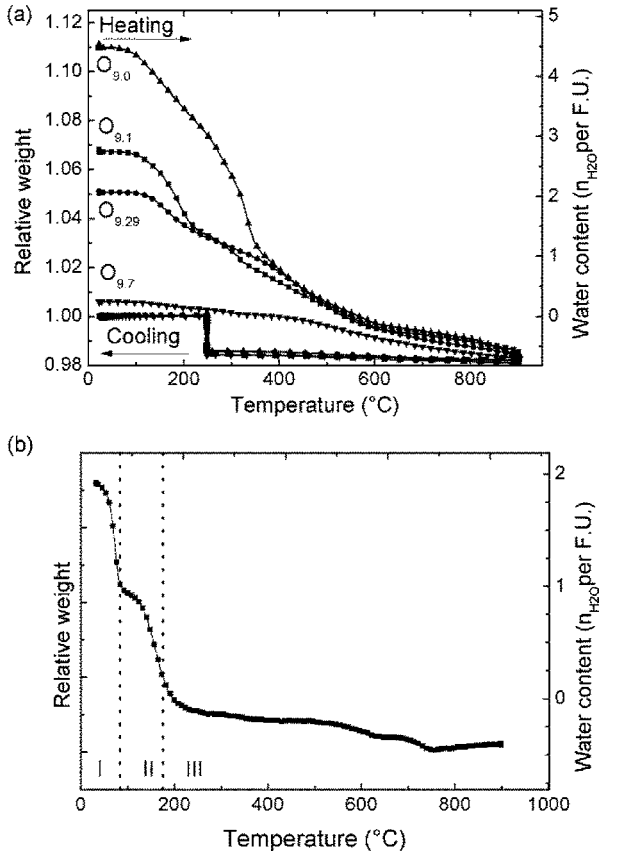

Figure 5. (a)Thermogravimetric data for samples subjected to accelerated hydration at 80 °C ($10-\delta$ = 9.7, 9.3, 9.1, and 9.0, symbolized by ▼, ●, ■ and ▲) measured upon heating in N_2 (10 °C/min). Upon subsequent cooling, the atmosphere was switched from N_2 to O_2 at 250 °C. After full oxidation, the samples were finally cooled to room temperature. (b)Thermogravimetric data for $O_{9.0}$ hydrated at ambient atmosphere and measured upon heating in N_2 at a rate of 1 °C/min. Different thermal loss regimes are indicated by Roman numbers.

some 200 °C. A small weight loss is further observed up to around 720 °C. The first weight loss below 80 °C corresponds to dehydration, while the second below 200 °C is due to dehydroxylation. The weight loss for some samples at higher temperature is due to reduction in N_2, relating to the formation of oxygen vacancies. This behavior resembles topotactic hydrolysis and hydration reactions reported for other RP phases.

The corresponding water loss is given by the right-hand axes of Figure 5. For the accelerated hydrated samples, the total loss corresponds to a maximum of $4.5H_2O$/f.u., whereas for samples hydrated at ambient, the loss corresponds to just around $2H_2O$/f.u. This difference in weight loss between the two conditions of hydration is striking. Hence, controlled decomposition reactions were performed in a special rig with strict control of atmosphere while monitoring gas products with a mass spectrometer. This proved unambiguously that during accelerated hydration, that is, above a water bath maintained at 80 °C, CO_2 is also absorbed from the air and is incorporated in the form of carbonate. This was further confirmed by FTIR experiments (see Supporting Information Figures II and III). Simultaneous hydration and carbonation has been recently shown to occur in $LiSr_2Ta_2O_7$ (though through reversible formation of Li_2CO_3).[29] Hence, pure hydration is only achieved

dx.doi.org/10.1021/ic300001s | Inorg. Chem. 2012, 51, 9181−9191

at mild conditions and fast reaction times. We will concentrate the remainder of our discussions on this category of products. For these samples, the TG data indicate loss of one water molecule above some 100 °C, which is attributed to hydroxyl groups; that is, $PrSr_3Co_{1.5}Fe_{1.5}O_{9-\delta}(OH)_2$ = $PrSr_3Co_{1.5}Fe_{1.5}O_{10-\delta}$ + H_2O. Regardless of the original oxygen nonstoichiometry of the RP3 precursor, the hydrated product contains two OH groups per f.u. For the range covered in Figure 5, three weight loss mechanisms are operative: (i) loss of crystal water; (ii) dehydroxylation, recombination, and departure of H_2O from the host; (iii) loss of O_2 along with creation of oxygen vacancies and reduction of the transition metal at the B site.

Regarding the aggressive hydration, we present to our knowledge for the first time evidence that combined hydration and carbonatation will occur for Fe/Co containing RP3 oxides via topotactic like reactions. This adds drastically to the complexity of the hydration mechanisms and is a topic for detailed studies of its own.

Structural Study of Topotactic Water Intercalation. The diffraction patterns in Figure 6 (see also Figure 1) reveal

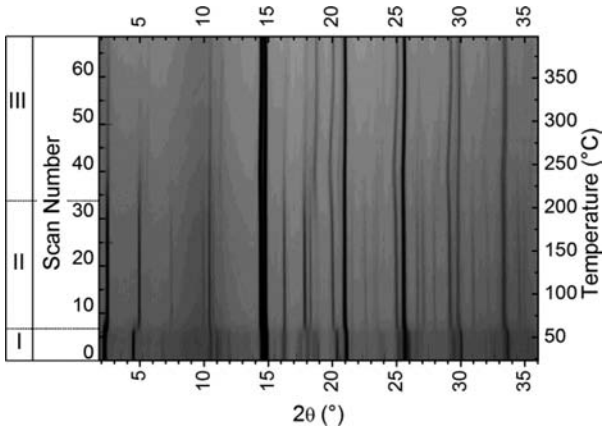

Figure 6. Powder XRD data as collected during calcination of $PrSr_3Co_{1.5}Fe_{1.5}O_9(OH)_2 \cdot H_2O$. Inverse gray scale picture of diffraction intensities versus temperature as collected with the MAR345 detector and transformed by means of the program FIT2D. Weight loss regimes are indicated by Roman numbers.

close relationships between the parent RP3-oxide and the various hydration products and indicate topotactic reactions during hydration and hydroxylation. The conversion of the hydrated oxide hydroxide into RP3-oxide was studied by means of SXRD. The investigated $PrSr_3Co_{1.5}Fe_{1.5}O_{8.9}$ (reduced at 250 °C in 10% H_2/Ar) was hydrated in ambient atmosphere for 7 days. The collected SXRD patterns in Figure 6 show phase transformations at some 70 and 170 °C and a change in thermal expansion around 230 °C. In the following, we denote the temperature windows as (I) for RT $\leq T \leq$ 70 °C, (II) for 70 $\leq T \leq$ 170 °C, and (III) for 170 $\leq T \leq$ 400 °C. In accordance with the TG data, a hydrated phase prevails in window I. Indexing of the diffraction data shows systematic reflection conditions; *hkl*, $h + k + l = 2n$, consistent with space group *I*2/*m*. The oxygen and water content of $PrSr_3Co_{1.5}Fe_{1.5}O_8(OH)_2 \cdot H_2O$ is proposed on the basis of the TG data. Crystal structure data are given below. In window II, TG data indicate a dehydrated oxide hydroxide phase, $PrSr_3Co_{1.5}Fe_{1.5}O_8(OH)_2$. The structure is orthorhombic, and no systematic extinctions were observed. The material is likely to crystallize in space group *Pmmm*. In window III, an RP3-oxide phase dominates with systematic reflection conditions *hkl*, $h + k + l = 2n$, in accordance with a body centered tetragonal structure; *I*4/*mmm*. Refined unit cell dimensions for the three phases are given in Table 2. The low values obtained

Table 2. Refined Unit Cell Parameters[a]

	hydrate	hydroxide	oxide
T (°C)	25	90	400
space group	*I*12/*m*1	*Pmmm*	*I*4/*mmm*
V (Å)	529.65(6)	243.2(2)	421.40(5)
a (Å)	3.8442(3)	3.876(2)	3.8614(2)
b (Å)	3.8493(3)	3.873(2)	3.8614(2)
c (Å)	35.808(3)	16.202(1)	28.262(2)
β (deg)	88.805(6)		
χ^2	0.661	0.81	0.28
Rp (%)	1.91	2.75	1.35
Rwp (%)	2.75	3.19	2.06

[a]Calculated standard deviations in parentheses.

for χ^2 (i.e., <1) presented in Table 2 are caused by a software artifact when using data collected with a 2D image plate detector and rebinned into 2θ vs intensity patterns. When such data is used in Fullprof, the program overestimates the esd's, thereby producing low GOF and χ^2 values.

The temperature dependence of the unit cell dimensions along with corresponding weight fractions upon heating were derived from Rietveld refinements and are displayed in Figure 7. Concerning the refinement procedure, each of the majority phases within the windows I, II, and III were first refined. While keeping the atomic parameters constant, the profile parameters, the phase fractions, the unit cell dimensions, and a global thermal parameter were refined. The hydrate oxide hydroxide and the oxide hydroxide phases were included in window I. At temperatures above the distinct transition at 70 °C, the oxide phase was added to the refinements. There is good correspondence between the thermogravimetric (Figure 5b) and in situ SXRD (Figure 8) data, respecting the different preparation and measurement strategies. The transformation around 70 °C from the crystalline hydrate to oxide hydroxide is distinct without intermediate stages. The conversion from oxide hydroxide to pure oxide occurs over a wide temperature range with the two phases coexisting. These phases with, respectively, *P* and *I* Bravais lattices are easily distinguishable. The data indicate that the oxide hydroxide decomposes in one step. However, the product appears not to be a pure oxide but is partly hydroxylated at intermediate temperatures, though having *I* symmetry. This is supported by the slow evolution of phase fractions above 250 °C and by the temperature dependencies of unit cell parameters. As seen from Figure 7, the unit cell expansion of the oxide *I*4/*mmm* phase is dominated by *c*-axis expansion. Possibly, the maxima in *c* and *V* at around 230 °C indicate the onset of dehydroxylation of the "oxide" formed in window III. Subsequent to this dehydroxylation, oxygen vacancies may form within a partly reduced RP-phase. These are in turn susceptible to filling up during reoxidation. Both scenarios may lead to unit cell contraction. Regarding the behavior of the unit cell dimensions of the hydrate in window I, one notices that the *a*, *b*, and *c* (*c*/2) axes approach those in window II, while the monoclinic angle remains relatively constant.

dx.doi.org/10.1021/ic300001s | *Inorg. Chem.* 2012, 51, 9181–9191

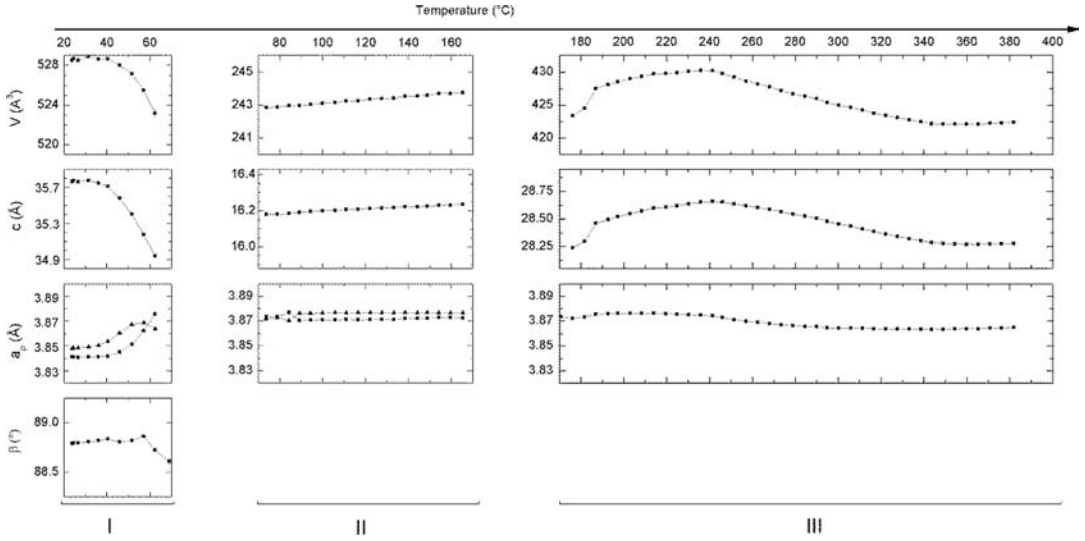

Figure 7. Temperature evolution of unit cell dimensions for hydrated oxide hydroxide, oxide hydroxide, and oxide variants of RP3 as derived from in situ XRD data during calcination of $PrSr_3Co_{1.5}Fe_{1.5}O_9(OH)_2{\cdot}H_2O$.

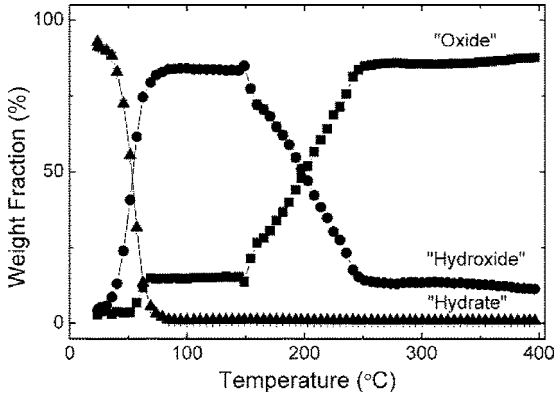

Figure 8. Weight fractions as derived from Rietveld refinements of in situ SXRD data.

Crystal structure data for the hydrate oxide hydroxide $PrSr_3Co_{1.5}Fe_{1.5}O_8(OH)_2{\cdot}H_2O$ in window I was derived from Rietveld refinements of SXRD data. Observed, calculated, and difference intensity profiles are shown in Figure 9. The pattern was successfully indexed on an *I*-centered monoclinic lattice

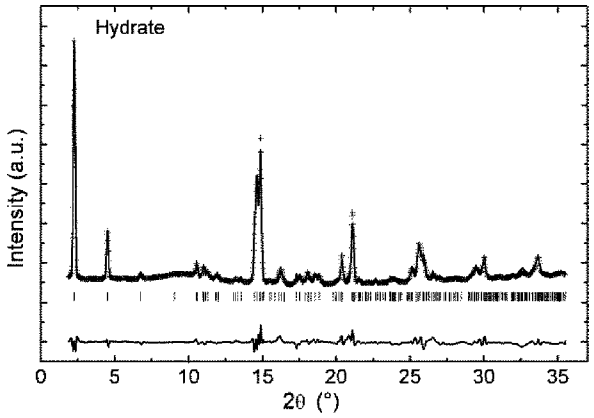

Figure 9. Observed, calculated, and difference intensity profiles from Rietveld refinement of room-temperature SXRD data for hydrated $PrSr_3Co_{1.5}Fe_{1.5}O_8(OH)_2{\cdot}H_2O$.

with dimensions a = 3.8462(3), b = 3.8492(3), and c = 35.834(3) Å and β = 88.847(7)°. The observed systematic reflection conditions, hkl, $h + k + l = 2n$, are consistent with space groups *I*2 (No. 5), *Im* (No. 8), and *I*2/*m* (No. 12). The highest symmetric space group *I*2/*m* was adopted. The structural model was developed by reducing Wyckoff positions of the tetragonal structure of $PrSr_3Co_{1.5}Fe_{1.5}O_{10-\delta}$. The proposed unit cell for the hydrate oxide hydroxide phase differs from that of hydrated $NdSr_3Fe_3O_9$ by the monoclinic angle. In the present case, the angle is located between the basal plane and the stacking axis of the perovskite layers, whereas for $NdSr_3Fe_3O_9$, it is located within the basal plane.[7] Also the latter description was currently inspected but was inferior both visually and in terms of reliability factors (that is, R_P, R_{wp}, and χ^2, respectively, calculated as 3.14, 6.00, and 3.13).

The refined atomic coordinates are given in Tables I, II, and II of the Supporting Information for the hydrated oxide hydroxide, the oxide hydroxide, and the oxide, respectively. Complementary powder neutron diffraction data for a deuterated sample is required for a detailed and complete structural analysis, notably for the positional and occupancy parameters for the oxygen atoms and water molecules. Such a study would furthermore allow a more detailed exploration of the calculated short distances between the oxygen atoms of the hydroxide and of the water molecule in the hydrated oxide hydroxide phase, a situation that could be an artifact induced by disorder, for example.

Water molecules were located based on Fourier difference, ΔF, maps. Figure 10 shows maps for sections at x = 0 and x = 1/2 within the *bc*-plane. These show additional electron density in the RS interlayer, that is, at (0, 0, 1/4) and (1/2, 1/2, 1/4). The water configuration is compatible with hydrogen bonds between the incorporated water molecules and O-atoms at separations below 3 Å, some being likely to be hydroxide anions.

Hydration Mechanism. The ability to hydrate is not a general feature for RP phases. It is therefore important to gain insight into underlying mechanisms and chemical prerequisites. The present study shows that hydration is fast for partly reduced $PrSr_3Co_{1.5}Fe_{1.5}O_{10-\delta}$ while hardly taking place for the fully oxidized phase, even at aggressive gas phase hydration

dx.doi.org/10.1021/ic300001s | Inorg. Chem. 2012, 51, 9181−9191

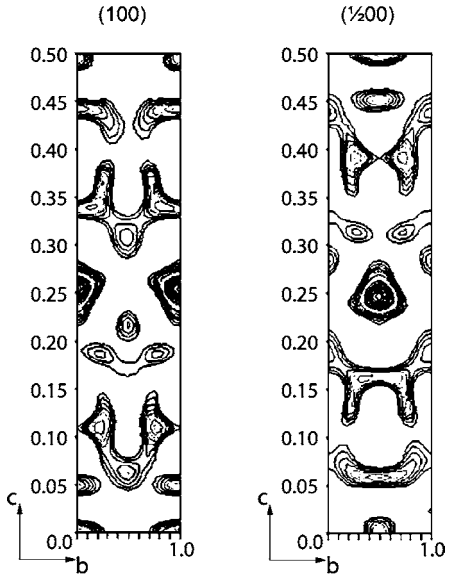

Figure 10. Sections of Fourier difference maps for the monoclinic structure of hydrated $PrSr_3Co_{1.5}Fe_{1.5}O_8(OH)_2{\cdot}H_2O$ as calculated from room-temperature SXRD data for the (100) and the ($^1/_2$00) planes.

conditions. At mild conditions, only water is incorporated; at aggressive conditions in air also carbonate is incorporated. As a general observation, the known RPs with hydration ability contain 3d-elements in high oxidation states and A-site cations with high basicity. It is not obvious which factors take dominating roles concerning thermodynamics and kinetics of hydration.

We take note of the following key observations (not all described above):

- Ability and capacity of hydration is at maximum for reduced samples with a considerable concentration of oxygen vacancies.
- Hydration yields direct formation of a hydrated oxide hydroxide without intermediates.
- At aggressive conditions (above water bath held 80 °C), carbonate is simultaneously incorporated. At mild conditions, pure hydrated oxide hydroxide is obtained. Upon prolonged exposure to ambient air at room temperature (weeks), the hydrated oxide hydroxide converts slowly into a carbonate-containing phase.
- Aqueous solutions turn basic when the reduced RP3 is added of concern for hydration. When a perovskite sample with similar chemical composition, oxidized and reduced, is subjected to water, no pH change is observed. Neither was any change observed for the relevant Pr_2O_3, Co_3O_4, or Fe_2O_3. In the case of SrO, a basic solution (pH $\approx$ 10) was obtained. No H_2 or O_2 evolution could be registered by MS.
- On addition of acid to the sample made upon accelerated hydration, CO_2 gas evolution appears immediately and is proven by mass spectrometry (see Supporting Information). No evolution of H_2 gas could be measured.
- The *a*-axis of the hydrated product and of the higher temperature oxide hydroxide is larger than for the fully oxidized sample. This may indicate a lower bond-order for the M−O bonds within the basal plane, that is, transition metals being in a partly reduced state. This is in line with bond valence calculations that give average valence of ca. 2.6 and ca. 3, respectively, for the B site in the central (B1) and outer perovskite blocks (B2). Detailed values are given in the Supporting Information.
- Upon high temperature treatment and dehydration, the material gains a higher weight in oxygen than in nitrogen atmosphere, indicating that the investigated hydrate sample is originally in a partially reduced state.

These observations can be considered in terms of possible chemical reactions:

1. full hydration in mild conditions:

$$A_4B_3O_9 + 2H_2O \leftrightarrow A_4B_3O_8(OH)_2{\cdot}H_2O$$

2. dehydration:

$$A_4B_3O_8(OH)_2{\cdot}H_2O \leftrightarrow A_4B_3O_8(OH)_2 + H_2O$$

3. partial dehydroxylation:

$$A_4B_3O_8(OH)_2 \leftrightarrow A_4B_3O_{8+x/2}(OH)_{2-x} + \frac{x}{2}H_2O$$

(oxide hydroxide)

4. full dehydroxylation:

$$A_4B_3O_{8+x/2}(OH)_{2-x} \leftrightarrow A_4B_3O_9 \quad \text{(reduced oxide)}$$

5. full reoxidation:

$$A_4B_3O_9 + \frac{1}{2}O_2 \leftrightarrow A_4B_3O_{10}$$

[note, $p(O_2)$ and temperature dependent]

6. oxidation of water:

$$H_2O \leftrightarrow \frac{1}{2}O_2 + 2e^- + 2H^+$$

[possibly by Ni(III), Co(III, IV), Fe(IV)]

7. reduction of water:

$$2H_2O + 2e^- \leftrightarrow H_2 + 2OH^-$$

[possibly by low-valent d-cations in the RP3]

8. carbonatization and hydration:

$$A_4B_3O_9 + yH_2O + CO_2 \rightarrow A_4B_3O_8(OH)_{2-x}(CO_3)_{x/2}{\cdot}yH_2O$$

9. carbonatization of hydrate:

$$A_4B_3O_8(OH)_2{\cdot}H_2O + CO_2 \rightarrow A_4B_3O_8(OH)_{2-x}(CO_3)_{x/2}{\cdot}yH_2O$$

This study shows the existence of a critical anion vacancy concentration for the hydration to take place, below which the material is shielded from water molecule attack. Based on these observations, we propose that O vacancies are essential for the hydration, in particular for the initial stage, at which water molecules are incorporated as OH groups with simultaneous protonation of oxide anions, probably situated in the RS block of the structure. The reduced RP3 of concern have been shown to have preferred locations of disordered O vacancies within the central part of the P blocks.[5] We suggest that the incorporated OH groups in the vacant O sites easily restructure with protons being transferred to the RS block, which would be consistent

dx.doi.org/10.1021/ic300001s | *Inorg. Chem.* 2012, 51, 9181−9191

with the significant *c*-axis expansion observed (for both the hydrate oxide hydroxide and the oxide hydroxide). The dissociation of the water molecules into OH^- and H^+ is therefore stimulated by the transition metal centers; the oxygen vacancies provide the accessible attack sites, while the possibility of atomic rearrangements provides means for ion transport within the layered structure. Therefore the hydration ability is directly related to the transition metal oxidation states. The O_9 stoichiometry of the oxide corresponding to an average M^{3+} (most probably a Co^{3+} and Fe^{3+} mixture) in an MO_{6-x} environment appears optimal for enhancing the reaction, while lower oxidation states appear to have an inhibiting effect, possibly indicating that M^{2+} species may be inactive for the described water dissociation.

The observed increase in pH upon hydration of the RP3, could be indicative of water reduction. However, the long *a*-axis of the hydrated and hydroxide phases suggests that no such RP3 oxidation has taken place. As alternative, we propose a slight RP3 decomposition in water (selective leaching of SrO), giving *inter alia* $Sr(OH)_2$ with solubility product $K_{sp} = 9 \times 10^{-10}$, which may explain the slightly basic solutions. The corresponding Pr, Fe, and Co oxides/hydroxides are less soluble. The lack of hydrogen or oxygen evolution, as monitored by MS, also speaks againts any redox reaction. Hence, we suggest that the oxidative/reductive power of the 3d-elements of the reduced RP3 is not a dominating factor with respect to hydration ability. The observations clearly show that carbonate formation leads to more stable products and becomes dominant at elevated temperatures and for long-term exposures to CO_2-containing atmospheres.

The involved RP3 phases contain typically quite basic A cations; that is, Ln and Sr. Let us therefore briefly consider the possibility of cation basicity as a dominant factor. Peña and Fierro[30] observed that reduced perovskites show enhanced ability to hydrate and suggested that water dissociation is favored by an acid–base-type reaction with the O^{2-} anion stabilizing the proton and the remaining hydroxyl group being stabilized by an oxygen vacancy in the structure. These considerations took advantage of the acidity assessments for probe molecules on reduced perovskites by Tejuca et al.[31] The concept of optical basicity, Λ,[32] for the Lewis acidity of oxides has found applications[33] in catalysis,[34] glasses,[35] and metallurgical slags[36] and mirrors the ability of the oxygen anion to donate electrons (CaO bond as Λ = 1 reference). For transition metal oxides (d^1–d^9), the optical basicity increases with coordination number (CN) and decreases for increasing cation charge (for CN = constant). On the basis of tabulated optical basicities,[33,37,38] one may calculate Λ for $M_i^{Zi+}{}_{Xi}O^{2-}{}_Y$ as[34]

$$\Lambda = \frac{1}{2Y}\sum_i X_i Z_i \Lambda_i$$

Values of Λ for selected binary oxides and $LnSr_3M_3O_{10-\delta}$ phases are given in Tables 3 and 4. We take note of the following: (i) the basicity is effectivily unchanged from Ln = La to Nd for $Ln_4M_3O_{10}$; (ii) the basicity increases with increasing nonstoichiometry (fixed Ln) $Ln_4M_3O_{10-\delta}$; (iii) the basicity increases with substitution of Co into the Fe site (M); and finally (iv) the basicity for $Ln_2Sr_2M_3O_{10}$ is smaller than that for $LnSr_3M_3O_{10}$. The $[AO]^{RS}$ layer can be considered as the interface between surfaces of two $[AMO_3]$ blocks. The latter contains more acidic Fe and Co sites, whereas the [AO] sites are more basic and may stabilize protons. It is tempting to postulate that spontaneous hydration has two prerequisites: (i) oxygen vacancies allowing facile absorption of water as precursor for hydroxyl groups and (ii) appropriate basicity allowing acid–base reactions to take place between water and the reduced RP oxide.

Table 3. Optical Basicities for Binary Oxides, Including Charge and Coordination of Cation

binary oxides	optical basicity	cation charge	coord. no.[a]
H_2O	0.4[33,34]	+1	1
CaO	1[33]	+2	6
SrO	1.1[33]	+2	6
La_2O_3	0.9609/0.9645[38]	+3	9/12
Nd_2O_3	0.9566/0.9608[38]	+3	9/12
Pr_2O_3	0.9575/0.9615[38]	+3	9/12
Fe_2O_3	0.66/0.74[37,39]	+3	4/6
FeO	0.76/1.00[37,39]	+2	4/6
CoO	0.77/0.98[37,39]	+2	4/6
Co_2O_3[c]	0.85[37,39]	+3	6

[a]Coordination number of the selected cation when applicable.

Table 4. Calculated Optical Basicities for Various RP Related Oxides

composition of RP phase	calculated optical basicity (comments)	ref[a]
$PrSr_3Co_{1.5}Fe_{1.5}O_{9.91}$	0.84 (CN 6/M^{3+})	this work
$PrSr_3Co_{1.5}Fe_{1.5}O_{9.5}$	0.88 (CN 6/M^{3+})	this work
$PrSr_3Co_{1.5}Fe_{1.5}O_{9.0}$	0.93(CN 6/M^{3+})	this work
$PrSr_3Co_{1.5}Fe_{1.5}O_{8.5}$	0.90 (50% CN 6 and 50% CN 4/Co^{2+}, Fe^{3+})	this work
$PrSr_3Co_{1.5}Fe_{1.5}O_{8.25}$	0.89 (0.5 CN 6 and 0.5 CN 4/M^{2+})	this work
$PrSr_3Co_{1.5}Fe_{1.5}O_8(OH)_2xH_2O$	0.77 (CN 6/M^{3+})	this work
$La_4Fe_{1.5}Co_{1.5}O_{10}$	0.9354(CN 6/M^{3+})[b]	IS
$Pr_4Fe_{1.5}Co_{1.5}O_{10}$	0.9335(CN 6/M^{3+})[b]	IS
$Nd_4Fe_{1.5}Co_{1.5}O_{10}$	0.9330(CN 6/M^{3+})[b]	IS
$La_4Fe_3O_{10}$	0.91 (CN 6/M^{3+})	IS
$La_4Co_3O_{10}$	0.96 (CN 6/M^{3+})	18

[a]IS indicates ideal structure, either hypothetical or taken from cited reference. [b]For clarity, the optical basicities were calculated using all significant digits from Table 3.

CONCLUSIONS

This work has aimed to shed more experimental light on hydration of Ruddlesden–Popper-type oxides based on studies of $PrSr_3Co_{1.5}Fe_{1.5}O_{10-\delta}$. Using the concept of the optical basicity, we suggest that the driving force is an acid–base-type reaction between the acidic water molecule (Λ = 0.4) and the RP3-type oxide (typically with Λ ≈ 0.9). However, there are additional prerequisites, the availability of oxygen vacancies for promoting uptake of water molecules appearing as the most essential one. This allows us to explain several current observations as well as behaviors reported in literature. First is the fact that, when sufficiently oxidized, a sample will not react spontaneously with water because it has no vacant sites for water absorption. Second, dependent on the A site composition (i.e., the ratio of lanthanide to alkaline earth), some RP phases may react more readily with water. Noteworthy, upon hydration at room temperature, the acid–

dx.doi.org/10.1021/ic300001s | Inorg. Chem. 2012, 51, 9181–9191

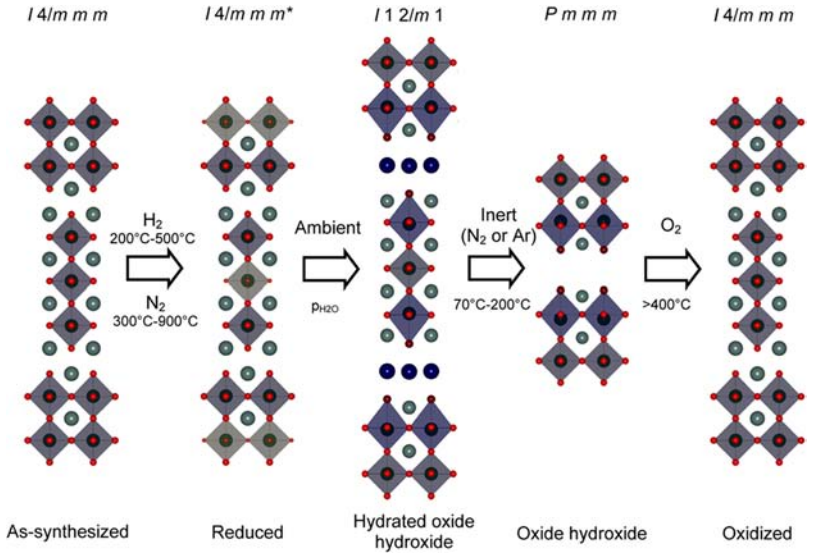

Figure 11. Schematic representation of the hydration process including conditions and crystal structures as obtained from refinement of SXRD data. Smaller atoms and lighter octahedra denote polyhedra with vacancies; darker octahedra and slightly bigger and darker atoms indicate polyhedra with OH groups.

base reaction that fills oxygen vacancies with hydroxyl groups is accompanied by the insertion of stabilizing water molecules within the $[AO]^{RS}$ layers. This reaction scheme is in real atmosphere subject to perturbations induced by the presence of carbon dioxide. These oxides, with high basicity in certain structural segments, show a pronounced tendency to preferably incorporate carbonate anions rather than hydroxyl anions, in particular at elevated temperature and upon prolonged exposure to CO_2-containing atmospheres.

The hydration reaction is currently proven to depend strongly on the oxygen nonstoichiometry of the RP3 phase. Indeed, oxygen vacancies are a prerequisite for the reaction to occur, while nearly fully oxygenated oxide samples remain inert under water-containing atmosphere. This suggests that RP-type oxides unstable under water-containing atmospheres may be stabilized by tuning of their oxygen stoichiometries, and vice versa. By means of SXRD, the location of interlayer water has been established. Upon heating, the loss of water and the conversion to an oxide hydroxide is established and supported by thermogravimetric analyses. Given the weakness of metal−H_2O interactions, the decomposition of the hydrate into oxide hydroxide is rapid whereas the opposite (acid−base) reaction is much slower. The intercalation of water molecules distorts the original tetragonal structure. The C_{2v} symmetry of H_2O groups may, along with effects due to directional hydrogen bonding, trigger this symmetry lowering. Upon heating, the monoclinic hydrate structure transforms to a primitive tetragonal oxide hydroxide structure, which finally reverts to the *I*-centered RP3 structure at high temperatures. As shown in Figure 11, the conversion from *I* (hydrate) to *P* (hydroxide) to *I* (HT phase) imposes repetitive shifting of the perovskite block (translated by 1/2a + 1/2b in the case of *I* symmetry when viewed along the *c*-axis) reflecting a sort of micaceous character of the crystal structure level during the transformation, possibly connected with the weaker hydrogen bonding in these layers. Therefore, a prerequisite for the topotactic hydration could be the layered character of the RP phases due to the AO−AO rock salt interlayer. Indeed, for parallel experiments with neighboring perovskite compositions, no hydration behavior could be observed.

There is no doubt that further knowledge on the driving force for spontaneous hydration would be necessary for becoming able to design novel layered oxide materials of RP-type. Their physical properties are expected to be significantly modified by the intercalation and proton donation to oxygen atoms. The present work is a contribution to such progress.

■ ASSOCIATED CONTENT

Ⓢ Supporting Information

The experimental setup for the hydration, details of the MS experiments, FTIR spectroscopy, and X-ray diffraction, tables of atomic coordinates and calculate bond valence parameters for the B sites, and structural data in CIF format. This material is available free of charge via the Internet at http://pubs.acs.org.

■ AUTHOR INFORMATION

Corresponding Author

*E-mail: helmer.fjellvag@kjemi.uio.no.

Present Address

[†]Université de Rennes I, UMR Sciences Chimiques de Rennes, F-35042 Rennes, France.

Notes

The authors declare no competing financial interest.

■ ACKNOWLEDGMENTS

This work was supported by the Research Council of Norway, Grant. No. 15818/S10 (NANOMAT), and the EU Marie Curie FP6 NOVELOX program, Grant No. MEST-CT-2004-514237. The authors acknowledge the assistance of the research team at the Swiss-Norwegian Beam Lines, ESRF, and thank Dr. S. Francis for fruitful discussions and help with the IR spectroscopy, as well as C. Sprung for his help and time with MS measurements

■ REFERENCES

(1) Ruddlesden, S. N.; Popper, P. *Acta Crystallogr.* **1957**, *10*, 538−539.

(2) Ruddlesden, S. N.; Popper, P. *Acta Crystallogr.* **1958**, *11*, 54−55.
(3) Dion, M.; Ganne, M.; Tournoux, M. *Mater. Res. Bull.* **1981**, *16*, 1429−1435.
(4) Byeon, S.-H.; Yoon, J.-J.; Lee, S.-O. *J. Solid State Chem.* **1996**, *127*, 119−122.
(5) Schaak, R. E.; Mallouk, T. E. *Chem. Mater.* **2002**, *14*, 1455−1471.
(6) Jantsky, L.; Norby, P.; Rosseinsky, M. J.; Fjellvåg, H. *Z. Kristallogr.* **2009**, *224*, 295−301.
(7) Pelloquin, D.; Hadermann, J.; Giot, M.; Caignaert, V.; Michel, C.; Hervieu, M.; Raveau, B. *Chem. Mater.* **2004**, *16*, 1715−1724.
(8) Pelloquin, D.; Barrier, N.; Flahaut, D.; Caignaert, V.; Maignan, A. *Chem. Mater.* **2005**, *17*, 773−780.
(9) Pelloquin, D.; Barrier, N.; Maignan, A.; Caignaert, V. *Solid State Sci.* **2005**, *7*, 853−860.
(10) Matvejeff, M.; Lehtimaki, M.; Hirasa, A.; Huang, Y. H.; Yamauchi, H.; Karppinen, M. *Chem. Mater.* **2005**, *17*, 2775−2779.
(11) Domen, K.; Yoshimura, J.; Sekine, T.; Tanaka, A.; Onishi, T. *Catal. Lett.* **1990**, *4*, 339−343.
(12) Takada, K.; Sakurai, H.; Takayama-Muromachi, E.; Izumi, F.; Dilanian, R. A.; Sasaki, T. *Nature* **2003**, *422*, 53−55.
(13) Lee, K.; Manthiram, A. *Chem. Mater.* **2006**, *18*, 1621−1626.
(14) Prado, F.; Armstrong, T.; Caneiro, A.; Manthiram, A. *J. Electrochem. Soc.* **2001**, *148*, J7−J14.
(15) Bréard, Y.; Michel, C.; Hervieu, M.; Studer, F.; Maignan, A.; Raveau, B. B. *Chem. Mater.* **2002**, *14*, 3128−3135.
(16) Brisi, C.; Rolando, P. *Ann. Chim.* **1969**, *59*, 385.
(17) Lee, J. Y.; Swinnea, J. S.; Steinfink, H.; Reiff, W. M.; Pei, S.; Jorgensen, J. D. *J. Solid State Chem.* **1993**, *103*, 1−15.
(18) Hansteen, O.; Fjellvåg, H. *J. Solid State Chem.* **1998**, *141*, 212−220.
(19) Hansteen, O. H.; Fjellvag, H.; Hauback, B. C. *J. Mater. Chem.* **1998**, *8*, 2089−2093.
(20) Karen, P. *J. Solid State Chem.* **2006**, *179*, 3167−3183.
(21) Nishi, T.; Toda, K.; Kanamaru, F.; Sakai, T. *Key Eng. Mater.* **1999**, *169*−*170*, 235−238.
(22) Hammersley, A. P.; Svensson, S. O.; Hanfland, M.; Fitch, A. N.; Hausermann, D. *High Pressure Res.* **1996**, *14*, 235−248.
(23) Rietveld, H. *J. Appl. Crystallogr.* **1969**, *2*, 65−71.
(24) Rodríguez-Carvajal, J. *Phys. B (Amsterdam, Neth.)* **1993**, *192*, 55−69.
(25) Barrier, N.; Pelloquin, D.; Nguyen, N.; Giot, M.; Bourée, F.; Raveau, B. *Chem. Mater.* **2005**, *17*, 6619−6623.
(26) Bréard, Y.; Raveau, B.; Pelloquin, D.; Maignan, A. *J. Mater. Chem.* **2007**, *17*, 2818−2823.
(27) Lehtimaki, M.; Hirasa, A.; Matvejeff, M.; Yamauchi, H.; Karppinen, M. *J. Solid State Chem.* **2007**, *180*, 3247−3252.
(28) Ito, J.; Frondel, C. *Am. Mineral.* **1967**, *52*, 1105−1109.
(29) Galven, C.; Fourquet, J.-L.; Suard, E.; Crosnier-Lopez, M.-P.; Le Berre, F. *Dalton Trans.* **2010**, *39*, 4191−4197.
(30) Pena, M.; Fierro, J. *Chem. Rev.* **2001**, *101*, 1981−2018.
(31) Tejuca, L. G.; Rochester, C. H.; Fierro, J. L.; Tascón, J. M. D. *J. Chem. Soc., Faraday Trans. 1* **1984**, *80*, 1089−1099.
(32) Duffy, J.; Ingram, M. *J. Am. Chem. Soc.* **1971**, *93*, 6448−6454.
(33) Duffy, J. *Geochim. Cosmochim. Acta* **1993**, *57*, 3961−3970.
(34) Bordes-Richard, E. *Top. Catal.* **2008**, *50*, 82−89.
(35) Duffy, J.; Ingram, M. *J. Non-Cryst. Solids* **1976**, *21*, 373−410.
(36) Duffy, J.; Ingram, M.; Sommerville, I. *J. Chem. Soc., Faraday Trans. 1* **1978**, *74*, 1410−1419.
(37) Lebouteiller, A.; Courtine, P. *J. Solid State Chem.* **1998**, *137*, 94−103.
(38) Zhao, X.; Wang, X.; Lin, H.; Wang, Z. *Phys. B (Amsterdam, Neth.)* **2007**, *392*, 132−136.
(39) Moriceau, P.; Lebouteiller, A.; Bordes, E.; Courtine, P. *Phys. Chem. Chem. Phys.* **1999**, *1*, 5735−5744.

dx.doi.org/10.1021/ic300001s | *Inorg. Chem.* 2012, 51, 9181−9191